

Hollow Structured Li_3VO_4 Wrapped with Graphene Nanosheets in-situ prepared by One-pot Template-free Method as Anode for Lithium-ion Batteries

Yi Shi ^{a,b}, Jia-Zhao Wang ^{b*}, Shu-Lei Chou ^b, David Wexler ^c, Hui-Jun Li ^d, Kiyoshi Ozawa ^e, Hua-Kun Liu ^b, Yu-Ping Wu ^{a*}

Supporting Information

1. Some evidence about the formation of the Li_3VO_4 microboxes

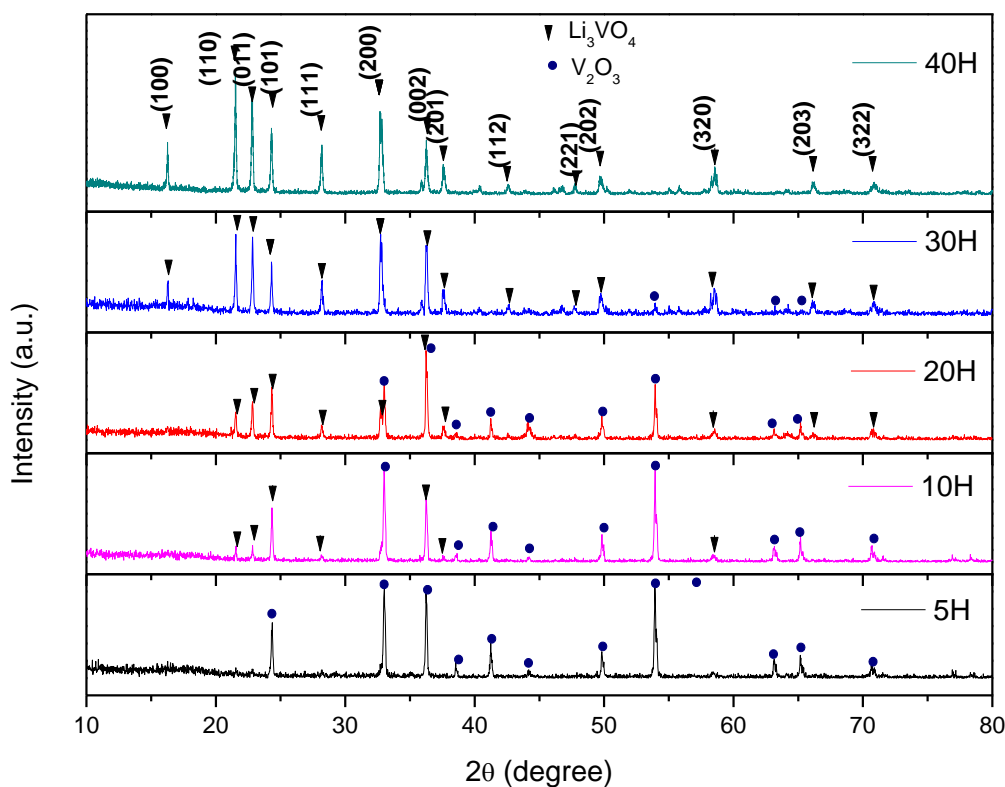


Figure S1 X-ray diffraction patterns (XRD) for the prepared Li_3VO_4 at different aging time.

To shed light on the formation mechanism of these novel Li_3VO_4 microboxes, their growth process has been followed by examining products harvested at different intervals of aging time. X-ray diffraction reveals the presence of both Li_3VO_4 and V_2O_3 structures after 10 h aging, with near complete transformation to Li_3VO_4 within 30-40 h, as shown in Figure S1.

The influence of the harvest time for LVO has also been investigated. After the hydrothermal treatment for 40 h, no impurity could be observed in the XRD pattern. It should be emphasized, however, that after the hydrothermal treatment for 40 h, the precipitate of pure Li_3VO_4 particles could have collected in the bottom of the vessel, while the dark colour of the solution means that there is still some unreacted V_2O_3 , which could have been removed by washing. On the other hand, LVO/G shows a transparent solution, which reflects the catalysis action of graphene oxide.

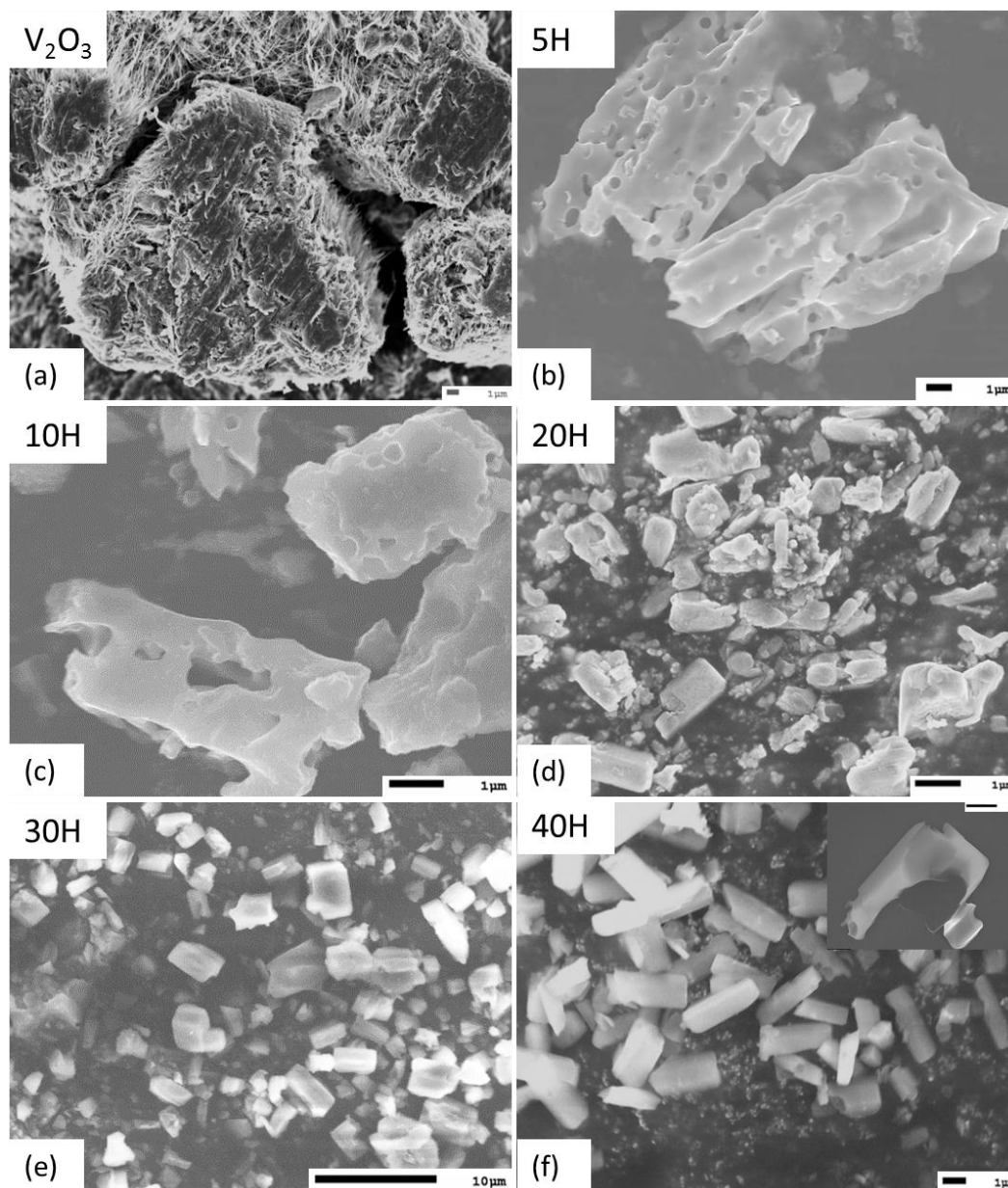


Figure S2 FESEM secondary electron micrographs of Li_3VO_4 products obtained after different aging time: (a) commercial V_2O_3 ; (b) 5 h; (c) 10 h; (d) 20 h; (d) 30 h; (f) 40 h, with the inset showing a single broken Li_3VO_4 microbox.

Figure S2 shows representative field emission scanning electron microscope (FESEM) secondary electron micrographs of the products obtained after various aging time. As shown in Figure S2a, the commercial as-

received V_2O_3 exhibits the morphology of irregularly shaped particles, around 20 μm in average diameter, with short nanowire or spike-like projections on the particle surfaces.

After 5 hours of hydrothermal treatment (Figure S2b), the particles have decomposed into slightly more faceted particles, with high interior and exterior porosity. Both the amount of facets and the size of both the interior pores and the exterior pores increased on increasing the aging time to 10 h (Figure S2c). The surfaces of the particles also became less smooth. This change in structure began the evolution of a particle shape which can be described as an irregular, partially hollow microbox with additional large surface holes.

Based on examination of the time-dependent formation of Li_3VO_4 microboxes, we propose that the microboxes are formed by the hollowing of the initial microrods by an oxygen-engaged oxidation process. The trace oxygen dissolved in solution may gradually oxidize V_2O_3 into VO_4^{3-} . Li_3VO_4 precipitated on the surface could ensure that the surfaces of the V_2O_3 cubes are effectively covered, which could make the surface of a V_2O_3 cube less reactive than the freshly exposed interior, once the pitting process has started. This is consistent with Scheme 1 in the main text.

2. Calculation the graphene amount from TG

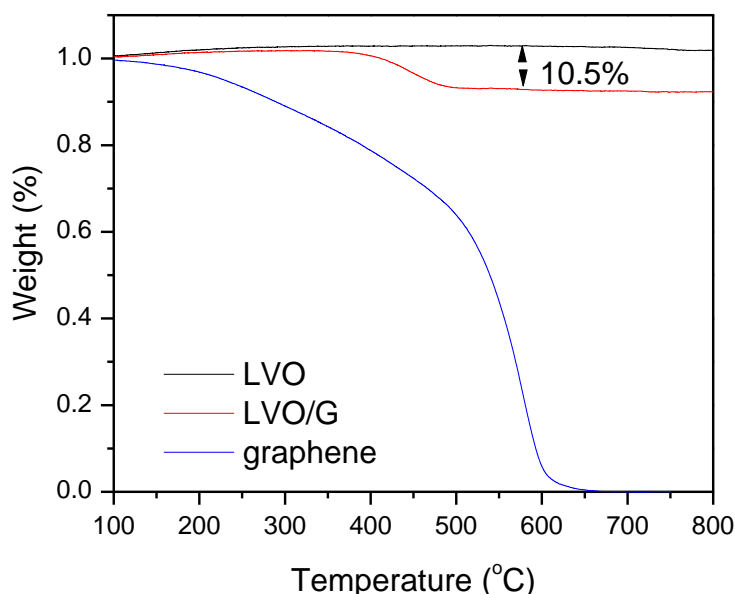


Figure S3 TGA curves of graphene, the Li_3VO_4 and the LVO/G composite.

The amount of graphene in the samples was estimated using a Mettler-Toledo thermogravimetric analysis/differential scanning calorimetry (TGA/DSC) 1 Star System from 100–800 $^{\circ}\text{C}$ at a rate of 5 $^{\circ}\text{C min}^{-1}$ in air flux (Figure S4). The results show a typical TGA curve of the Li_3VO_4 /graphene composite sample along with those of samples of Li_3VO_4 and graphene. The difference in weight between the Li_3VO_4 and the Li_3VO_4 /graphene after the oxidation could be translated into the amount of graphene in the Li_3VO_4 /graphene composite. By this method, the amount of graphene in the LVO/G composite was estimated to be approximately 10.5 wt. %.

3. Cyclic voltammograms of the Li_3VO_4 and the LVO/G composite in the first five cycles

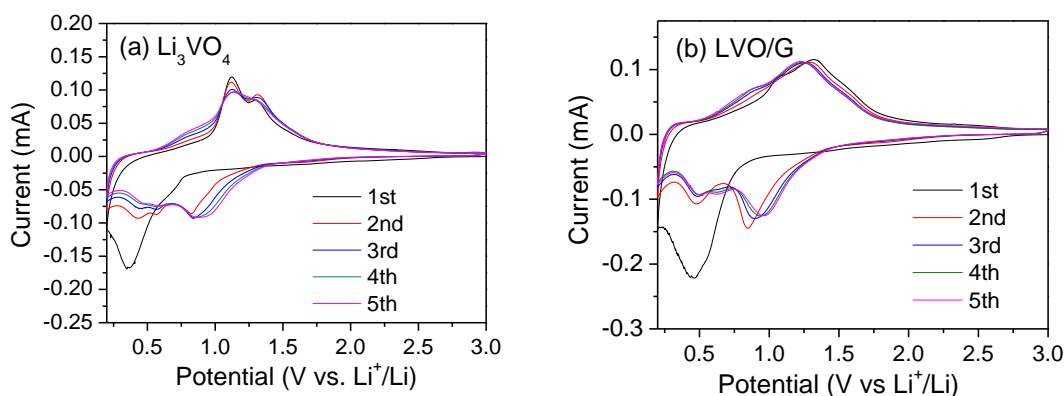


Figure S4 Cyclic voltammograms in the first five cycles at a scan rate of 0.1 mV s^{-1} of (a) the Li_3VO_4 and (b) the LVO/G composite.

The cyclic voltammograms (CVs) of the Li_3VO_4 and the LVO/G composite for the first five cycles are shown in Figure S4. The structure of Li_3VO_4 is composed of corner-sharing VO_4 and LiO_4 tetrahedra. Lithium ions are expected to reversibly insert into empty sites in the structure.¹ Although further oxidation of V^{5+} in Li_3VO_4 is hard to achieve, reduction to V^{3+} by the insertion of lithium into the structure is possible through the charging process. The insertion of Li^+ into Li_3VO_4 can be interpreted by an initial solid-solution step and then a two-phase mechanism.² The theoretical capacity is calculated to be 394 mAh g^{-1} , in accordance with $x = 2$ in $\text{Li}_{3+x}\text{VO}_4$.²

The peaks correspond to the small inflections in the typical charge/discharge curves in Figure 3a in the main text. This irreversible behavior in the initial CV cycles of the LVO/G composite is consistent with the results of the charge and discharge tests, and this might be related to the form of the SEI films and the insertion instability in the initial stage. Comparing the LVO/G composite with the bare Li_3VO_4 , it shows that the composite exhibits higher current density and better overlapping. These results suggest that the $\text{Li}_3\text{VO}_4/\text{graphene}$ electrodes have better kinetic properties, and it is considered that this phenomenon is mainly due to the graphene in the composite.

4. Typical discharge and charge profiles between different voltage limits

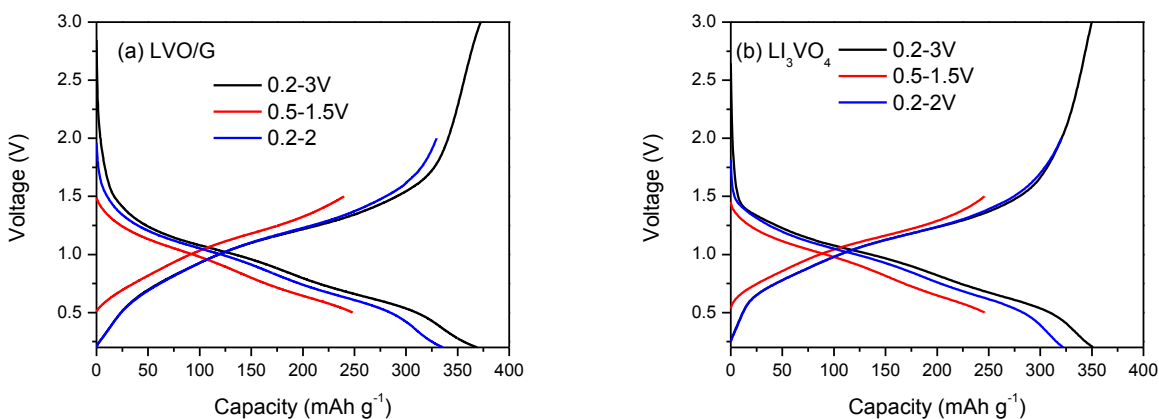


Figure S5 Typical discharge and charge profiles of (a) LVO/G and (b) Li_3VO_4 at the current density of 20 mA g^{-1} between different voltage ranges measured by a Land Battery Tester.

The voltage range of all the electrical performance in the manuscript and supporting information is 0.2-3 V. This voltage range is similar to the reference ² and easy to compare with. The charge/discharge profile of different voltage range is shown in Figure S6. Shrinking the voltage range would slightly reduce the capacity.

5. Some characteristics of the Li_3VO_4 and the LVO/G composite after cycling

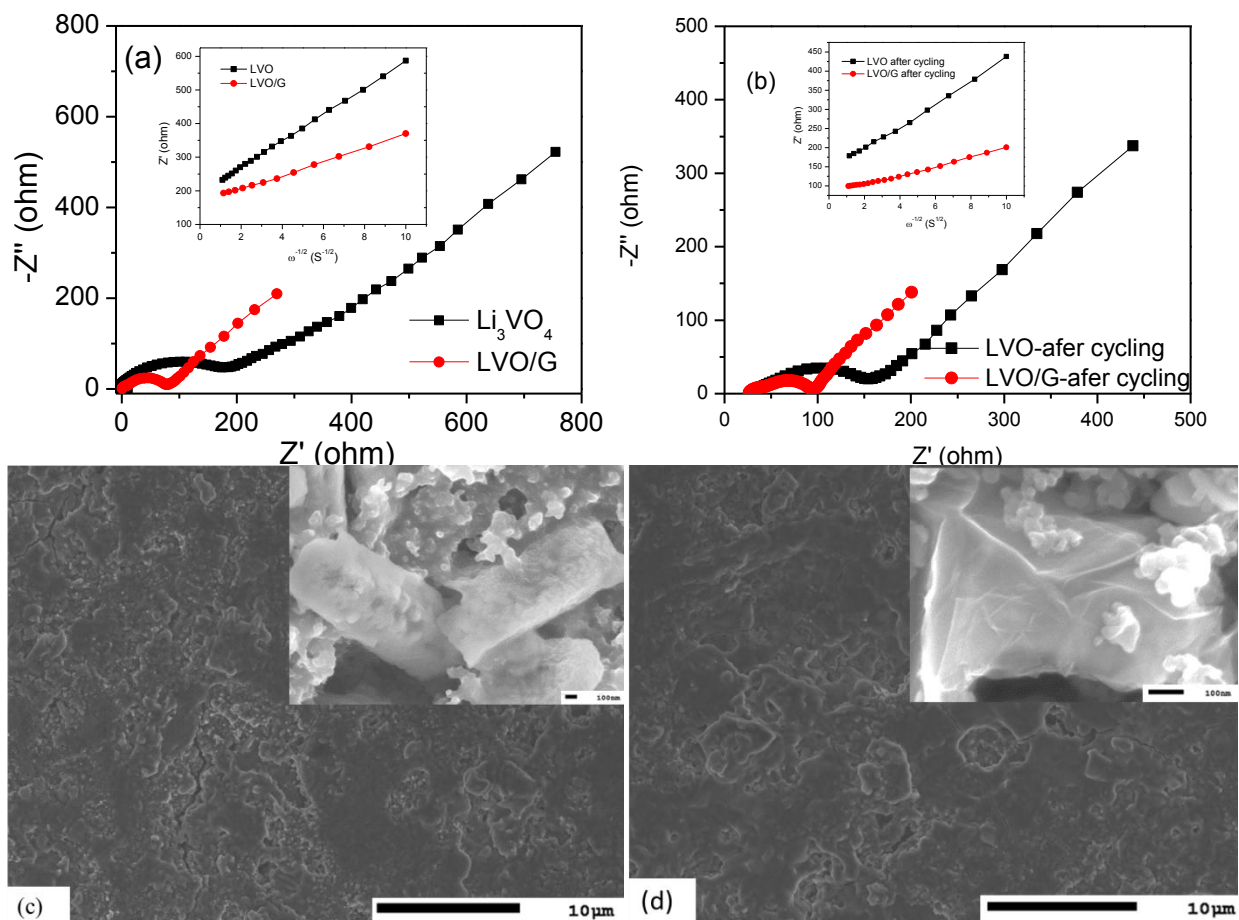


Figure S6 Some characteristics of the Li_3VO_4 and the LVO/G composite after cycling: (a) Nyquist plots of the Li_3VO_4 and the LVO/G composite after 5 cycles at an anode potential of 0.75 V (vs Li^+/Li) (inset); (b) Nyquist plots (EIS spectra) of the Li_3VO_4 and the LVO/G composite after 30 cycles at an anode potential of 0.75 V (vs Li^+/Li) (inset); (c) SEM micrograph of the Li_3VO_4 after 30 cycles with the inset showing two Li_3VO_4 microboxes; (d) SEM micrograph of the LVO/G composite after 30 cycles with the inset showing a single Li_3VO_4 microbox wrapped with graphene.

The properties of the Li_3VO_4 and the LVO/G composite after cycling have been investigated by electrochemical impedance spectroscopy (EIS) and SEM (Figure S5). The EIS spectra of the LVO and LVO/G electrodes were collected after charge–discharge for 5 cycles or 30 cycles at the potential of 0.75 V. The Nyquist plots (Figure S5a and 5b) show two compressed semicircles in the high to medium frequency range of each spectrum, which describe the charge transfer resistance (R_{ct}) for these electrodes, and an approximately 45° inclined line in the low-frequency range, which could be considered as Warburg impedance (Z_W), which is

associated with the lithium-ion diffusion in the bulk of the active material. The first compressed semicircle is related to the SEI film, and the high-frequency intercept of the second semicircle is related to the uncompensated resistance (R_u), while the diameter of the second semicircle is related to the charge transfer resistance (R_{ct})³. After simulating the whole circle of the second compressed semicircle for both samples, the values of R_{ct} for the Li_3VO_4 and the LVO/G composite electrodes after 5 cycles were calculated to be 211 and 80 Ω , respectively, while the values of R_{ct} for the Li_3VO_4 and LVO/G electrodes after 30 cycles were calculated to be 166 Ω and 72 Ω , respectively. All the resistance of the Li_3VO_4 and the LVO/G composite decreased after 30 cycles, which could be caused by the slow permeation of electrolyte into the hollow structure.

The EIS spectra can also be used to calculate the lithium diffusion coefficient according the equations (2 and 3) in the main text.

According to the linear fitting, the slope of the real part of the complex impedance versus $\omega^{-1/2}$ at various temperatures at an anodic potential of 0.75 V (vs. Li^+/Li) for the Li_3VO_4 and the LVO/G composite electrodes after 5 cycles is 39.3 and 20.1, respectively. The lithium diffusion coefficients are calculated to be 2.37×10^{-13} and $9.18 \times 10^{-13} \text{ cm}^2 \text{ s}^{-1}$ for the Li_3VO_4 and the LVO/G composite, respectively, at 25 $^\circ\text{C}$.

After 30 cycles, the slope of the real part of the complex impedance of the Li_3VO_4 and the LVO/G composite at the anode potential of 0.75 V (vs. Li^+/Li) is 29.1 and 11.4, respectively. The lithium diffusion coefficients are calculated to be 4.32×10^{-13} and $2.82 \times 10^{-12} \text{ cm}^2 \text{ s}^{-1}$ for the Li_3VO_4 and the LVO/G composite, respectively, at 25 $^\circ\text{C}$. The lithium diffusion coefficients of the Li_3VO_4 and the LVO/G composite have increased after 30 cycles, which could also be caused by the slow permeation of the electrolyte into the hollow structure.

A large particle size is unfavourable for the relaxation of such structural stress, and thus the large Li_3VO_4 particles may crack into several small particles after the insertion/deinsertion of Li^+ . A similar observation has been reported in previous research.² The cracking may cause the increasing resistance. According to the SEM micrograph, neither electrodes shows obvious cracks, which may be attributed to the hollow structure, which reduces the lattice pressure during charge/discharge.

6. Comparison of the charge and discharge curves of the LVO/graphene composite and the LVO/graphite composites

The charge and discharge curves for the composites of Li_3VO_4 microboxes/graphene and Li_3VO_4 microboxes/graphite were tested, and the results are showed in Figure S7.

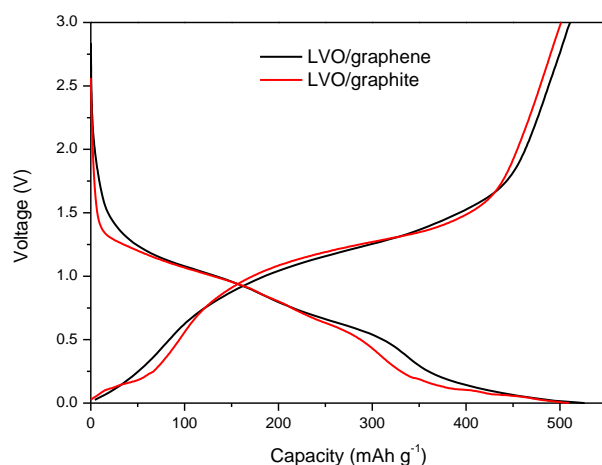


Figure S7 Typical discharge and charge profiles of LVO/graphene and LVO/graphite at the current density of 20 mA g^{-1} between different voltage limits measured by a Land Battery Tester.

The LVO/graphite electrode exhibits a much higher capacity below 0.2 V.

REFERENCES:

1. Kim, W.-T.; Jeong, Y. U.; Lee, Y. J.; Kim, Y. J.; Song, J. H. *Journal of Power Sources* **2013**, 244, (0), 557-560.
2. Li, H.; Liu, X.; Zhai, T.; Li, D.; Zhou, H. *Advanced Energy Materials* **2013**, 3, (4), 428-432.
3. Murugan, A. V.; Muraliganth, T.; Manthiram, A. *Journal of the Electrochemical Society* **2009**, 156, (2), A79-A83.